




Article

A Preliminary Study on the Identification of Genes Involved in Lignification in the Endocarp of Bared-Nut Walnut (*Juglans regia* L.) in Xinjiang, China

Shangqi Yu ^{1,2,3,†}, Jiazhi Fu ^{3,4,†}, Qian Ye ^{1,2,3}, Pengyu Wu ^{3,4}, Jianping Bao ^{2,3,4}, Haifang Hu ⁵, Zhongzhong Guo ^{2,3,4}, Rui Zhang ^{2,3,4,*} and Qiang Jin ^{2,3,4,*} 

¹ College of Life Science and Technology, Tarim University, Alar 843300, China; leypin@163.com (S.Y.); 13779585900@163.com (Q.Y.)

² Xinjiang Production & Construction Corps Key Laboratory of Protection and Utilization of Biological Resources in Tarim Basin, Alar 843300, China; guozhong88@foxmail.com (Z.G.)

³ The National-Local Joint Engineering Laboratory of High Efficiency and Superior-Quality Cultivation and Fruit Deep Processing Technology on Characteristic Fruit Trees, Alar 843300, China; 18890970103@163.com (J.F.)

⁴ College of Horticulture and Forestry, Tarim University, Alar 843300, China

⁵ Institute of Landscape Architecture, Xinjiang Academy of Forestry, Urumqi 830063, China

* Correspondence: zhrghs@163.com (R.Z.); qiangjin@taru.edu.cn (Q.J.); Tel.: +86-152-9250-2816 (R.Z.)

† These authors contributed equally to this work.

Abstract: This study focused on the “Xinlu” walnut and explored the molecular regulatory mechanism of lignin synthesis in the endocarp, aiming to explain the formation of bared-nut walnuts through morphological, metabolomic, and transcriptomic techniques. It was found that the synthesis of lignin, cellulose, p-coumaryl alcohol, and sinapyl alcohol was severely inhibited in the pulpy-hue (PUH) of the endocarp. We obtained 14 modules (gene sets) significantly correlated with the lignification factor (LIG) and 1548 hub genes. Additionally, we identified a MEplum3 module involved in endocarp lignin synthesis, primarily participating in phenylalanine biosynthesis and the lignin biosynthetic process. Meanwhile, we constructed a gene co-expression network for the MEplum3 module and identified a key hub gene for lignin synthesis—*JrCAD10*. Among the different tissues of “Xinlu”, the expression level of *JrCAD10* in the scleritic-hue (SCH) was significantly higher than in other tissues, with a relative copy number (RCN) of 3.2. However, *JrCAD10* expression was severely suppressed in the PUH. The suppression of *JrCAD10* expression led to the inhibition of lignin monomer synthesis, which further resulted in inhibited lignin synthesis, thus forming the bared-nut walnut. Our findings provide new insights into understanding the regulation of lignin synthesis and offer a possible explanation for the formation of bared-nut walnuts.

Keywords: walnut; bared-nut; sinapyl alcohol; lignin monomers



Citation: Yu, S.; Fu, J.; Ye, Q.; Wu, P.; Bao, J.; Hu, H.; Guo, Z.; Zhang, R.; Jin, Q. A Preliminary Study on the Identification of Genes Involved in Lignification in the Endocarp of Bared-Nut Walnut (*Juglans regia* L.) in Xinjiang, China. *Horticulturae* **2024**, *10*, 487. <https://doi.org/10.3390/horticulturae10050487>

Academic Editor: Yuepeng Han

Received: 31 March 2024

Revised: 21 April 2024

Accepted: 6 May 2024

Published: 8 May 2024



Copyright: © 2024 by the authors. Licensee MDPI, Basel, Switzerland. This article is an open access article distributed under the terms and conditions of the Creative Commons Attribution (CC BY) license (<https://creativecommons.org/licenses/by/4.0/>).

1. Introduction

The walnut (*Juglans regia* L.), a gem within the Juglandaceae family, has a good reputation and is widely cultivated globally. Walnut cultivation is exceptionally prevalent in the United States, Iran, and China, which constitute the three major pillars of the worldwide walnut industry [1,2]. Walnut fruit boasts extensive application prospects and market demand. The green walnut husk, known as “Qinglongyi” in its immature state, occupies a significant position as a medicinal herb in traditional Chinese medicine, boasting a rich history spanning nearly a thousand years in China [3]. As modern medical research continues to expand, scientists have uncovered many antitumor-active ingredients within the green walnut husk, exhibiting remarkable antitumor effects and presenting new avenues and potential therapeutic strategies in cancer treatment [4]. Walnut shells are a type of biomass material with significant application potential, and they can be used

to extract shell polysaccharides that clear hydroxyl radicals, superoxide anion radicals, and 2,2-diphenyl-1-picrylhydrazyl (DPPH) radicals [5]. Their derivatives can also be powerful natural adsorbents for removing heavy metals, hazardous compounds, and harmful substances from synthetic industrial dyes [6]. Walnut kernels, as the essence of walnuts and a nutritional treasure of nature, supply essential unsaturated fatty acids such as omega-3 and omega-6, which the human body cannot produce but are indispensable for health. They also contain an abundance of vitamins E and B; minerals such as zinc, selenium, calcium, and magnesium; and potent polyphenol (gallic acid, catechin, p-hydroxybenzoic acid, etc.) antioxidants [7,8]. These comprehensive nutrients fulfill people's daily nutritional requirements and are widely used in processed food, pharmaceuticals, and health products, making them essential components of a healthy lifestyle in modern times [9–11].

In recent years, deep-processed walnut products have garnered widespread market interest because of their exceptional nutritional value and diverse applications. This prevailing trend has propelled the walnut industry's shift from conventional preliminary processing toward the more technologically sophisticated realm of deep processing. Nonetheless, the challenge of cracking the hardy shells of walnuts during the processing phase remains a significant technical hurdle impeding the industry's progress.

The walnut fruit consists of a husk, hard shell, seed coat, and seed. Its outermost layer is a fleshy green husk. During the middle to late stages of development, a hard shell forms inside the husk, and the seed coat closely adheres to the surface of the seed. The seed and seed coat are enclosed at the center of the fruit by the formed hard shell [12]. The walnut pericarp comprises the green husk and the white fleshy tissue that closely adheres to the inner side of the husk. The husk's outer surface is the walnut's exocarp, while the green tissue beneath this outer surface is the mesocarp. The white fleshy tissue is defined as the endocarp, and, during the late stage of fruit development, only the outer one-third to two-thirds of the endocarp plays a crucial role in forming the walnut shell [13].

The maturation of walnut shells is accompanied by a significant thickening of the cell walls, primarily due to the increased lignin, cellulose, and hemicellulose contents. Lignin, as the main component of the cell walls, initially begins to deposit within the pectin network between cells and then gradually extends throughout the entire cell wall. The increase in lignin content plays a crucial role in the mechanical strength and durability of the walnut shell. The other major cell wall components, cellulose and hemicellulose, provide rigid support and maintain the cell wall's structural integrity during the walnut shell's maturation process [14–16].

Previous research findings have uncovered key genes in the phenylpropanoid metabolism pathway, such as *C3H*, *CCOAOMT*, and *CAD* [17–19]. Activating or inhibiting these genes can regulate the structure and content of lignin. Although these discoveries have provided a broad perspective on regulating lignin biosynthesis, a clear switch that can completely turn lignin synthesis on or off has yet to be found.

In this study, we primarily explored the hub genes related to the development of the walnut endocarp at the transcriptome level. Transcriptome and metabolome data from the five developmental stages of the walnut endocarp were utilized to identify key hub genes associated with endocarp development. We identified several key hub genes related to the lignin biosynthetic pathway during the developmental period of the walnut endocarp. Our preliminary research on these key hub genes allows us to speculate on the gene regulatory network of walnut endocarp development. It also provides a new perspective for uncovering the developmental switches involved in walnut shell formation in the future.

2. Materials and Methods

2.1. Plant Materials and Treatments

Xinlu, an exceptionally unique bared-nut walnut cultivar, is characterized by under-developed or minimally lignified regions of the endocarp. Its female flowers reach peak bloom between April 12th and 20th, and the fruits mature in early to mid-September. The

fruit shape resembles an ellipse, with a slightly concave top and a flat base; the average weight of a single fruit is approximately 15.8 g, and the average kernel yield is around 49.86%. Additionally, the average thickness of its nutshell is 1.75 mm, and the kernel can be easily separated [20]. This particular variety is cultivated in the fields of the second team at the Wensu County Walnut Farm in the Xinjiang Uyghur Autonomous Region, China.

Preliminary experiments indicate that the walnut cultivar “Xinlu” enters the lignification stage of its endocarp starting from the 50th day after full bloom. This is followed by a rapid synthesis phase of endocarp lignin that lasts for approximately two weeks, then a slow accumulation phase of endocarp lignin for another two weeks, and, finally, a second synthesis phase of endocarp lignin that also lasts for about two weeks, thus completing the entire endocarp lignification process. Therefore, five fruit developmental stages were carefully chosen, specifically, 50, 64, 71, 78, and 92 days following the peak bloom of the walnut tree (designated as StA, StB, StC, StD, and StE, respectively). At each developmental stage, 50 walnut fruits were randomly harvested. From these, the endocarp of 45 walnut fruits was carefully separated into two distinct regions, including the scleritic-hue (SCH) region, the hardened, shell-like area in which lignification has taken place, and the pulpy-hue (PUH) region, the unlignified fleshy portion.

Meanwhile, 3 biological replicates were obtained for each sample, with each biological replicate consisting of 15 randomly selected walnut fruits. Thus, 27 biological experimental sample materials were obtained in this study. The experimental materials were stored in a -80°C cryogenic chamber for subsequent total RNA extraction, transcriptome sequencing, and metabolomic measurements.

2.2. Visualization of Lignin in Walnut Endocarp via the Color Reaction

The lignin visualization method of the walnut inner pericarp was optimized based on our previous description [21]. The optimized method makes the experimental operation more convenient, and the lignin visualization is excellent. The specific steps are as follows: (1) prepare an alcohol–hydrochloric acid solution with a volume ratio of 1:1 using 95% ethanol and concentrated hydrochloric acid; (2) dissolve phloroglucinol in the alcohol–hydrochloric acid solution to prepare a 5% phloroglucinol–alcohol–hydrochloric acid mixed stain; (3) place the sliced (material) walnut fruit in the staining solution for 2–3 min, during which lignin will be specifically stained pink in an acidic environment; (4) use tweezers to remove the sliced material from the staining solution, and blot the surface of the material with absorbent paper to remove excess stain; and (5) finally, collect image data using optical imaging instruments, such as a stereo microscope or a direct camera.

2.3. Measurement of Lignin, Cellulose, and Hemicellulose Content

The lignin content of 27 samples was determined using a Lignin Content Assay Kit (Solarbio, Beijing, China). The samples were dried to a constant weight at 60°C , ground into a fine powder, and sieved through a 30–50 mesh sieve. Approximately 3 mg of each sample was weighed and transferred into a 1.5 mL Eppendorf tube. The subsequent experimental steps followed the kit’s operational protocol. Finally, the optical density (OD) of the samples was measured spectrophotometrically, and the lignin content was calculated using the provided formula.

A Cellulose (CLL) Content Assay Kit (Solarbio, Beijing, China) was employed to determine the cellulose content. At the same time, a Hemicellulose Content Assay Kit (Solarbio, Beijing, China) was used to measure the hemicellulose content. The sample pretreatment for both assays was conducted as described in the lignin content determination protocol.

2.4. Total RNA Extraction and qRT-PCR Analysis

According to the manufacturer’s protocol, the total RNA was extracted from the walnuts using an E.Z.N.A. Plant RNA Kit (OMEGA, Norcross, GA, USA). The quality of the extracted total RNA was assessed and confirmed to be suitable. The high-quality total RNA was reverse-transcribed into cDNA using an EasyScript One-Step gDNA Removal and

cDNA Synthesis SuperMix Kit (TRANSGEN, Beijing, China). The resulting cDNA from 27 walnut samples was utilized as a template, and quantitative reactions were performed on a QuantStudio™ 5 Real-Time PCR Instrument (384-Well Block) system. We used the 18S ribosomal gene *LOC121245754* of walnut as an internal reference gene to normalize gene amplification data (ΔC_t). The relative copy number (RCN) was calculated using the formula $RCN = 2^{-\Delta\Delta C_t}$, where $\Delta C_t = C_t$ (target gene) – C_t (internal reference gene) and $\Delta\Delta C_t = \Delta C_t$ (target gene) – ΔC_t (reference gene). All primers used in this study were synthesized by Tsingke (Tsingke Biotechnology Co., Ltd., Xi'an, China). The information is included in Table S1.

2.5. Metabolomics Analysis of Lignin Synthesis

MetWare (Wuhan, China, <http://www.metware.cn/>, accessed on 10 August 2023) analyzed the components and contents of lignin metabolites in the walnuts. Qualitative and quantitative analyses of the lignin metabolites were performed using UPLC-MS/MS technology. The frozen endocarp samples were ground and extracted with a 70% aqueous methanol solution. Following centrifugation and solid-phase extraction, the samples were filtered through a 0.22 μ m membrane for subsequent analysis. A Waters ACQUITY UPLC HSS T3 C18 column was used for sample separation, with a mobile phase comprising water containing 0.04% acetic acid and acetonitrile. Mass spectrometry detection was performed on an API 4500 Q TRAP system, utilizing an MRM analysis in both positive- and negative-ion modes to monitor the ion transitions of specific metabolites for a qualitative analysis. A data analysis, encompassing a peak area comparison, fold-change calculation, and statistical testing, was conducted using analyst software to ensure the accuracy and reliability of the quantitative results.

2.6. LncRNA Sequencing and Data Analysis

The RNA sequencing of the walnut samples was successfully carried out by BGI (located in Shenzhen, China, at <https://www.bgi.com/>, accessed on 5 November 2022). Initially, ribosomal RNA was effectively eliminated using a Ribo-Zero™ rRNA Removal Kit to minimize background interference. Next, under specified conditions, the purified RNA underwent fragmentation, synthesizing single-stranded cDNA using random primers and reverse transcriptase from a TruSeq® Stranded kit. Subsequently, double-stranded cDNA was formed with the help of DNA Polymerase I and RNaseH. Notably, dUTP replaced dTTP to prevent further amplification of the second cDNA strand. Ultimately, the cDNA received an “A” tail and was subsequently joined with sequencing adapters. After the necessary amplification and purification steps, the resulting LncRNA library was ready for high-throughput sequencing on the HiSeq4000 platform.

SOAP v1.5.2 [22] software was used to eliminate rRNA reads. In contrast, fastQC v0.12.1 software cleaned up dirty raw reads containing adapters, excessive Ns, or a high proportion of low-quality bases, resulting in clean reads for subsequent analysis. The Walnut 2.0 genome (https://www.ncbi.nlm.nih.gov/datasets/genome/GCF_001411555.2/, accessed on 8 May 2023) was used as the reference for aligning and assembling the read data. HISAT2 v2.2.1 [23] and StringTie v2.1.7 [24] software were employed for this alignment and assembly process, while Bowtie2 v2.4.4 [25] and RSEM v1.3.3 [26] were utilized for a quantitative analysis of the assembled transcripts. After obtaining the novel transcripts, we used CPC2 v1.0.1 [27], txCdsPredict v1.0.1, and CNCI [28] prediction software, along with the Pfam (http://ftp.ebi.ac.uk/pub/databases/Pfam/current_release/, accessed on 20 November 2022) [29] database, to predict their coding potential and distinguish between mRNAs and LncRNAs. To better understand gene functions, we annotated the assembled mRNAs using various databases, including NR, NT, GO, KOG, KEGG, and SwissProt.

We employed the WGCNA v1.72 software package to perform a weighted gene co-expression network analysis (WGCNA) on the walnut transcriptome data. Pearson's correlation coefficient (Cor), Student's *t*-test (*p*-value), gene significance (GS), and mod-

ule membership (MM) metrics were used to identify potential hub genes linked to the target trait.

2.7. Statistical Analysis and Data Visualization

Metascape (<https://metascape.org/gp/index.html#/main/step1>, accessed on 23 March 2024) was used for GO and KEGG enrichment analyses of the hub genes. Statistical significance (Student's *t*-test) was calculated using the Stats v4.2.3 software package. Data visualization was achieved using TBtools v2.37.0.0 [30], ggplot2 v4.2.3, Cytoscape v3.9.1, and GSDS v2.0 (<http://gsds.gao-lab.org/>, accessed on 17 March 2024) [31].

3. Results

3.1. Differences in Lignin, Cellulose, and Hemicellulose Contents between the PUH and SCH of “Xinlu” Walnuts

Lignin can undergo a chemical reaction with a lignin-specific staining solution, causing the lignified tissue to exhibit a red color. The saturation of this red color is positively correlated with the lignin content in the lignified tissue. At the StA stage, the endocarp of “Xinlu” walnuts begins its process of lignification, initiating the biosynthesis and deposition of lignin in cells (Figure 1A, StA). From StA to StE, the saturation of red gradually increases. This red color first appears in the endocarp regions at the apex and base of the fruit, subsequently emerging in the endocarp area in the middle of the fruit. This indicates that the lignification of the endocarp is a gradually intensifying process, with lignification first commencing in the endocarp regions at the top and base of the fruit. The lignification of the endocarp area in the middle of the fruit lags behind that of the top and base regions (Figure 1A, Ls).

We determined the contents of cellulose, hemicellulose, and lignin, the three main components of the endocarp, in the PUH and SCH of “Xinlu” walnuts during five stages (from StA to StE). The results show that the variation range of the cellulose content in the PUH remained between 22.06 mg/g and 27.01 mg/g, showing a relatively stable trend. However, the cellulose content in the SCH fluctuated between 8.68 mg/g and 12.29 mg/g. By comparing the two sets of data, it could be clearly observed that the cellulose content in the PUH was significantly higher than that in the SCH (Figure 1C). From StA to StB, the hemicellulose content in the PUH increased slightly from 58.07 mg/g to 60.82 mg/g, while in the SCH, it rapidly climbed to 83.59 mg/g. During the transition from StB to StD, the hemicellulose content in the PUH underwent a significant decrease, dropping from 60.82 mg/g to 35.41 mg/g. Meanwhile, the hemicellulose content in the SCH also decreased from 83.59 mg/g to 62.89 mg/g. However, from StD to StE, the hemicellulose content in the PUH rebounded to 59.06 mg/g, while in the SCH, it increased sharply to 129 mg/g (Figure 1D). At StA, the lignin content was at its lowest level, specifically at 40.5 mg/g, but it climbed to its peak at StE, reaching 401.7 mg/g. From StA to StB, the lignin content in the PUH gradually increased from 40.5 mg/g to 151 mg/g. However, in the SCH, the lignin content rose sharply to 349.2 mg/g, which was 2.3 times the content in the PUH during the same period. From StB to StE, the lignin content in the PUH fluctuated slowly between 151 mg/g and 201.35 mg/g, while in the SCH, its content remained stable, fluctuating between 349.2 mg/g and 401.7 mg/g. It is worth noting that the mass of lignin in the SCH accounted for up to 40.83% of the total dry matter mass, whereas in the PUH, this proportion only accounted for up to 20.72% (Figure 1B).

We found that there is a short period of rapid lignin accumulation (from StA to StB stage) and a longer period of slow accumulation (from StB to StE stage) in the endocarp of “Xinlu” walnuts. Additionally, significant differences in cellulose, hemicellulose, and lignin contents emerged from the developmental stage of StA to StB in both PUH and SCH, with the most pronounced differences observed in the lignin content. Therefore, we speculate that the formation of PUH in the endocarp of “Xinlu” walnuts may be due to the severe inhibition of lignin biosynthesis.

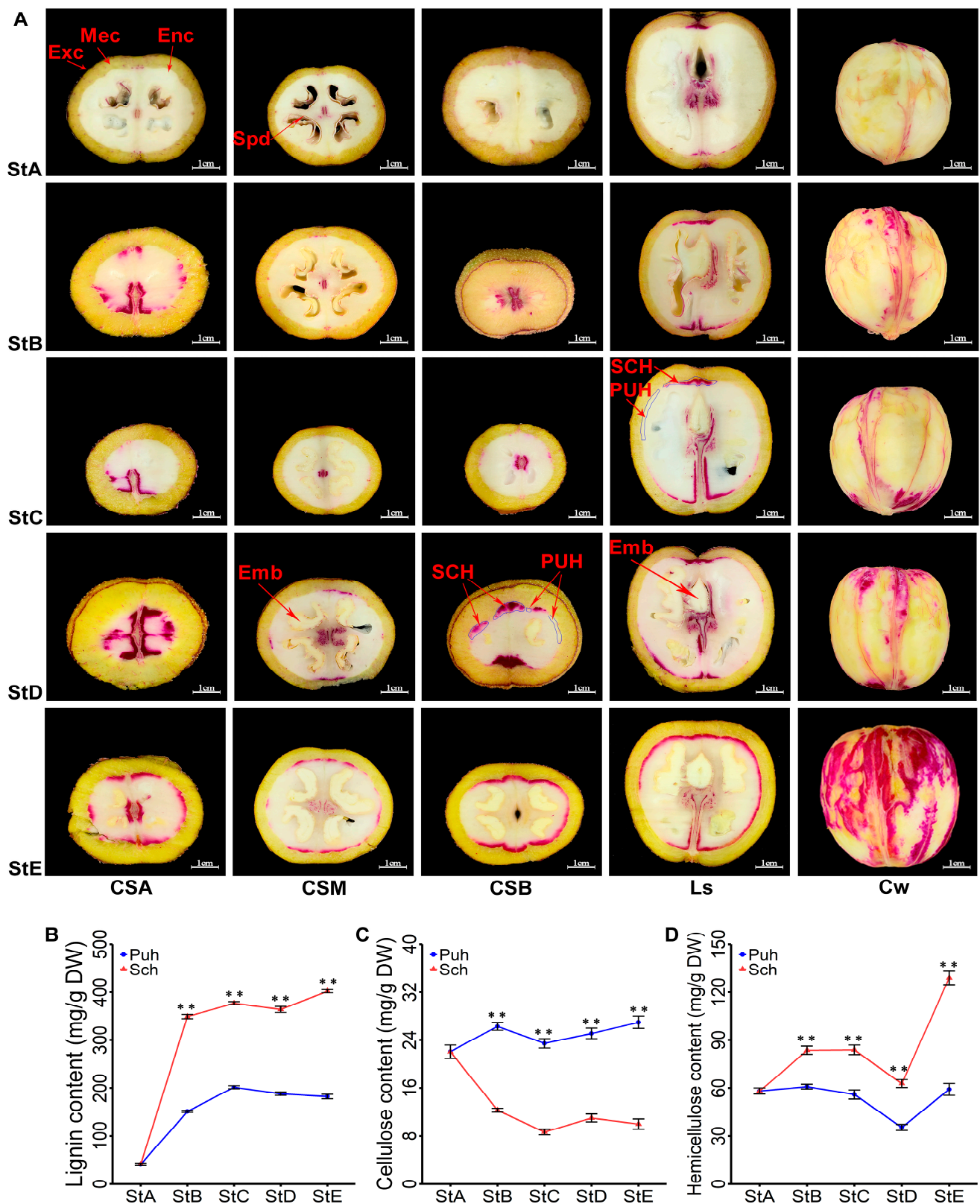


Figure 1. The contents of lignin, cellulose, and hemicellulose in the PUH and SCH of "Xinlu" walnuts. Panel (A) shows the phenotypic characteristics of lignin staining in "Xinlu" walnuts during the five stages from StA to StE. StA means 50 days after peak blooming (DAF), StB means 64 DAF, StC means 71 DAF, StD means 78 DAF, and StE means 92 DAF. The structure of the walnut fruit is mainly divided into five parts: exocarp (Exc), mesocarp (Mec), endocarp (Enc), sporoderm (Spd), and embryo (Emb).

The abbreviations CSA, CSM, and CSB designate the cross-sectional profiles corresponding to the walnut fruit's apical, median, and basal regions. The acronyms Ls and Cw correspond to the longitudinal sectional view and the perspective of the complete whole walnut fruit, respectively. Scale bars are 1 cm. Panels (B–D) depict the contents of lignin, cellulose, and hemicellulose. The data represent the mean \pm SD. The asterisk denotes a significant difference between the walnut PUH and SCH in the same period, as determined using Student's *t*-test. ** $p < 0.01$. Error bars represent the standard error of 3 biological replicates. Scleritic-hue (SCH) is the hardened, shell-like area where lignification has taken place, and pulpy-hue (PUH) is the unligified fleshy portion. DW means the dry weight of the endocarp of "Xinlu" walnuts.

3.2. Quantification of the 14 Metabolites in the Phenylpropanoid Biosynthesis Pathway of the PUH and SCH of "Xinlu" Walnuts

We found that lignin is the most dominant component in the dry matter of the endocarp of "Xinlu" walnuts. The lignin content in the PUH was approximately 20% lower than that in the SCH (Figure 1B), which is a noteworthy and intriguing change.

The biosynthesis of lignin can be subdivided into two parts, including the upstream common phenylpropanoid biosynthetic pathway and the downstream specific lignin biosynthetic pathway. To explore which substances altered during lignin biosynthesis lead to the inhibition of lignin biosynthesis in the PUH, we employed a UPLC-MS/MS analysis to determine the content of 14 metabolites related to lignin biosynthesis in the PUH and SCH of the endocarp of "Xinlu" walnuts. Based on the Wilcoxon test and fold change (Fc), where $Fc = \text{Log}_2(\text{SCH/PUH})$, we screened for metabolites related to lignin biosynthesis that exhibited significant differences between the PUH and SCH of the endocarp of "Xinlu" walnuts, using the criteria of $|Fc| \geq 1$ and $p < 0.05$.

The upstream common phenylpropanoid biosynthetic pathway mainly involves the biosynthesis of six acids. According to the statistical analysis, from StB to StE, the differences in the contents of L-phenylalanine, ferulic acid, and caffeic acid between the PUH and SCH were not significant. At StC, the content of p-coumaric acid in the PUH was significantly lower than that in the SCH ($Fc=3.189$), but there was no significant difference in the content of p-coumaric acid between the PUH and SCH at StB, StD, and StE. The content of sinapic acid in the SCH was significantly higher than that in the PUH at StB and StD (Fc 1.228 and 1.031, respectively). From StB to StE, the cinnamic acid content in the SCH was significantly higher than that in the PUH, with Fc values of 2.416 and 2.721, and 1.777 and 1.886, respectively. In the downstream-specific lignin biosynthetic pathway, among the eight metabolites, significant differences in the contents of caffeic aldehyde, 4-hydroxy-3-methoxycinnamaldehyde, p-coumaraldehyde, p-coumaryl alcohol, sinapinaldehyde, and sinapyl alcohol were observed between the PUH and SCH. At StE, there were also significant differences in the content of caffeyl alcohol and coniferyl alcohol between the PUH and SCH (Table 1, Supplementary Material Table S2). It is worth noting that from StA to StE, the relative content of sinapyl alcohol increased from 5220 to 12,300 in the SCH, but sinapyl alcohol was not detected in the PUH (Table 1). In the PUH, the biosynthesis of two lignin monomers, p-coumaryl alcohol and sinapyl alcohol, which are necessary for lignin biosynthesis in the endocarp of "Xinlu" walnuts, was significantly reduced, especially the biosynthesis of sinapyl alcohol, which was almost completely inhibited. This suggests that the blockage of sinapyl alcohol biosynthesis may be an important factor leading to the severe inhibition of lignin biosynthesis in the PUH.

Table 1. Comparisons of contents of 14 metabolites in the PUH and SCH of “Xinlu” walnuts.

Compounds	The Fold Change in SCH and PUH in the Endocarp of “Xinlu” Walnut at Different Developmental Stages			
	StB	StC	StD	StE
L-Phenylalanine	0.004	−0.488	−0.580	−0.309
Cinnamic acid	2.416	2.721	1.777	1.886
p-Coumaric acid	−0.343	−3.189	−0.170	−0.355
Ferulic acid	−0.908	−0.952	0.219	0.178
Caffeic acid	−0.311	0.388	0.707	0.261
Sinapic acid	1.228	0.919	1.031	−0.029
Caffeic aldehyde	0.100	−1.572	−1.706	−1.607
p-Coumaraldehyde	3.242	4.063	4.327	3.908
4-Hydroxy-3-methoxycinnamaldehyde	1.719	1.539	2.244	2.103
Sinapinaldehyde	3.705	4.690	4.034	1.803
Coniferyl alcohol	0.038	0.488	0.601	1.178
Caffeyl alcohol	−0.948	−0.130	−0.081	1.129
p-Coumaryl alcohol	3.498	5.482	4.855	3.483
Sinapyl alcohol	13.350 *	14.502 *	13.916 *	14.586 *

* Means not detected in the PUH. StA means 50 days after peak blooming (DAF), StB means 64 DAF, StC means 71 DAF, StD means 78 DAF, and StE means 92 DAF.

3.3. Lignification-Related Hub Genes in the PUH and SCH of “Xinlu” Walnuts

Based on the analysis of lignin metabolomics and the quantification of lignin, cellulose, and hemicellulose contents, it was found that the biosynthesis of sinapyl alcohol in “Xinlu” walnuts exhibited significant differences between the PUH and SCH. Consequently, we conducted transcriptome sequencing on 27 samples from PUH and SCH across five developmental stages from StA to StE to elucidate the key hub genes and the molecular regulatory networks involved in sinapyl alcohol biosynthesis. After filtering, assembling, and annotating the completed sequencing raw data, we obtained 39,991 genes and 68,690 transcripts. Based on the criteria of a non-zero FPKM in each sample and an average FPKM greater than one, we ultimately screened and obtained an expression matrix for 15,479 genes. These genes were subsequently used as input data for a WGCNA analysis. By applying the thresholds of $|Cor| > 0.5$ and $p < 0.01$, 14 modules (gene sets) significantly correlated with LIG were extracted (Figure 2A). Additionally, 1548 hub genes were identified within these 14 modules based on $|MM| > 0.8$ and $|GS| > 0.5$. To understand the biological functions of these hub genes in endocarp development, we performed GO and KEGG enrichment analyses using Metascape. The results indicated that these hub genes were primarily enriched in biological metabolic pathways related to plant cell wall development, such as phenylalanine metabolism, phenylpropanoid biosynthesis, and cell wall formation (Figure 2B).

A walnut gene encoding cinnamyl alcohol dehydrogenase (CAD) was identified within the MEplum3 module and designated as *JrCAD10* (MXL.25669). To further explore the biological processes involving the hub genes in the MEplum3 module, we conducted GO and KEGG enrichment analyses on the 128 hub genes within this module using Metascape. The results indicated that the hub genes in the MEplum3 module were significantly enriched in pathways related to phenylalanine, tyrosine, and tryptophan biosynthesis, as well as lignin biosynthetic processes, cytoskeleton organization, plant cell wall organization, and biogenesis (Figure 2C). This suggests that the hub genes in the MEplum3 module play a predominant role in the biosynthesis of lignin in the endocarp of walnuts.

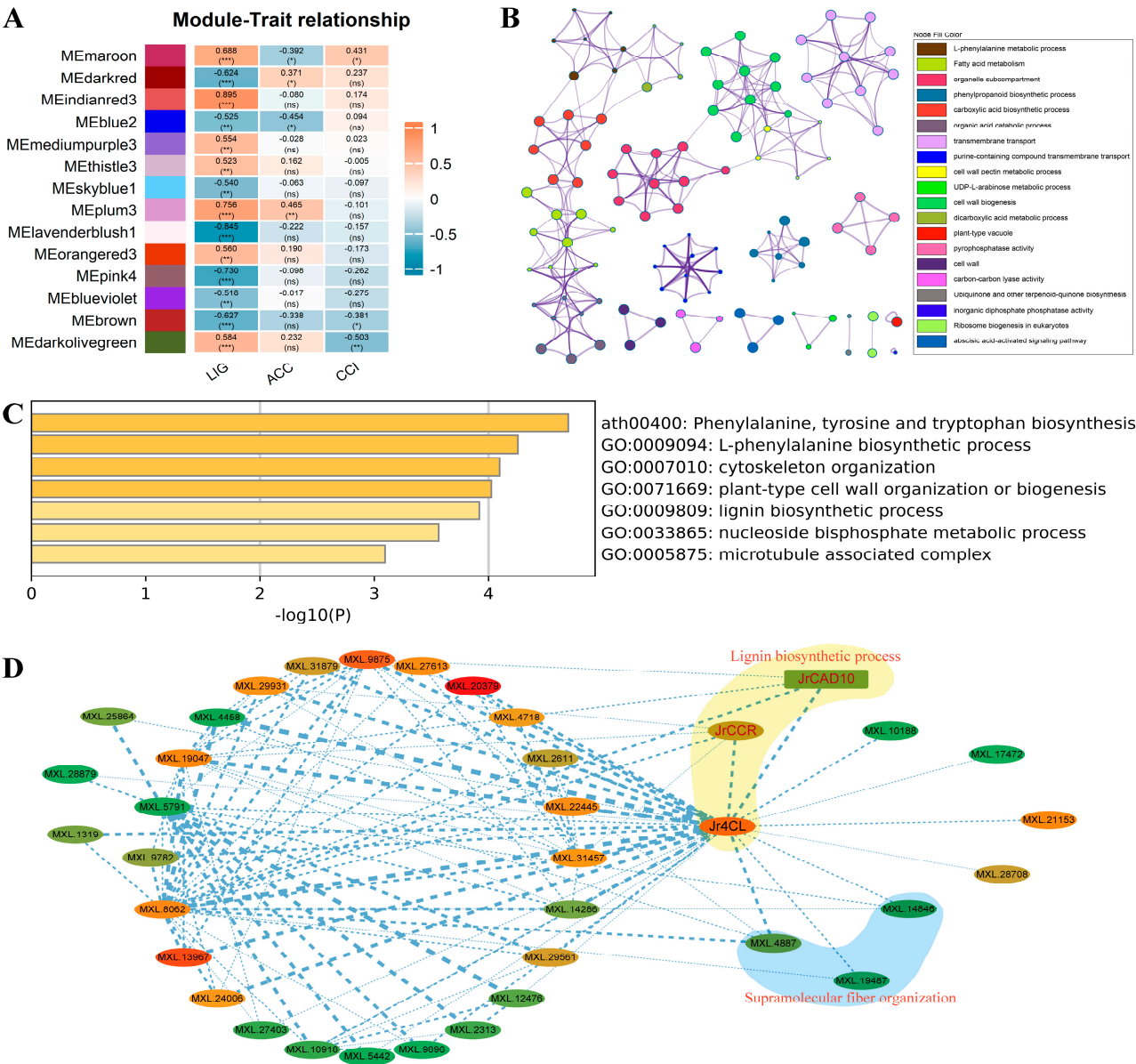


Figure 2. WGCNA of RNA–Seq data. **(A)** A heatmap depicting the correlations between 14 gene sets and three phenotypic traits. The lignification factor (LIG), acid compound conversion factor (ACC), and cinnamic acid and coumaric acid interconversion factor (CCI) were obtained through a PCA analysis of 14 metabolites to elucidate the primary biological processes in the phenylpropanoid pathway. The heatmap grid values represent the Pearson correlation coefficients between the gene sets and traits, with “ns” indicating a p -value > 0.05 , “*” indicating $p > 0.01$, “**” indicating $p > 0.001$, and “***” indicating $p \leq 0.001$. **(B)** Enrichment network of hub genes within the 14 modules based on GO and KEGG analyses. Each term is represented by a circle node, the size of which is proportional to the number of input genes that fall under that term, and the color represents its cluster identity (i.e., nodes of the same color belong to the same cluster). Terms with a similarity score > 0.3 are linked by an edge (the thickness of the edge represents the similarity score). **(C)** The GO and KEGG enrichment bar graphs of hub genes in the MEplum3 module. **(D)** The co-expression network of key hub genes in the MEplum3 module. In this network, the nodes’ fill color represents the fold change in the average expression levels of the genes between scleritic-hue (SCH) and pulpy-hue (PUH). When the weight between two nodes is greater than or equal to 0.25, they are connected by a dashed line, and the width of the dashed line indicates the strength of the weight.

To investigate other genes that are co-expressed with *JrCAD10*, we obtained the scale-free gene co-expression matrix from the MEplum3 module. A weight threshold (weight > 0.25) was set to eliminate weak connections, resulting in a co-expression matrix of 37 genes. We visualized this matrix using Cytoscape v3.9.1 software. The results showed that the genes *MXL.8062*, *MXL.5791*, and *Jr4CL* (*MXL.23751*) exhibited higher network node degrees, thereby emerging as key nodes in the entire co-expression network (Figure 2D). After a comprehensive analysis, we obtained three key hub genes with co-expression relationships in the lignin biosynthesis pathway during the development of walnut endocarp, as follows: *Jr4CL*, *JrCCR*, and *JrCAD10*. These three genes are important for the synthesis of three lignin monomers, namely, p-coumaryl alcohol, coniferyl alcohol, and sinapyl alcohol, and they are crucial for the final lignin synthesis and assembly.

3.4. Analysis of Gene Structure, Evolution, Chromosomal Localization, and Protein Conservation of Walnut *JrCAD* Genes

Based on the analysis of transcriptome sequencing data and the reference genome, we identified 11 *JrCAD* family members in “Xinlu” walnuts. We found that *JrCAD1*, *JrCAD10*, and *JrCAD11* were located on chromosomes 1, 13, and 16 of walnut, respectively; *JrCAD2*–*JrCAD5* were located on chromosome 2; and *JrCAD6*–*JrCAD9* were located on chromosome 8 (Figure 3A).

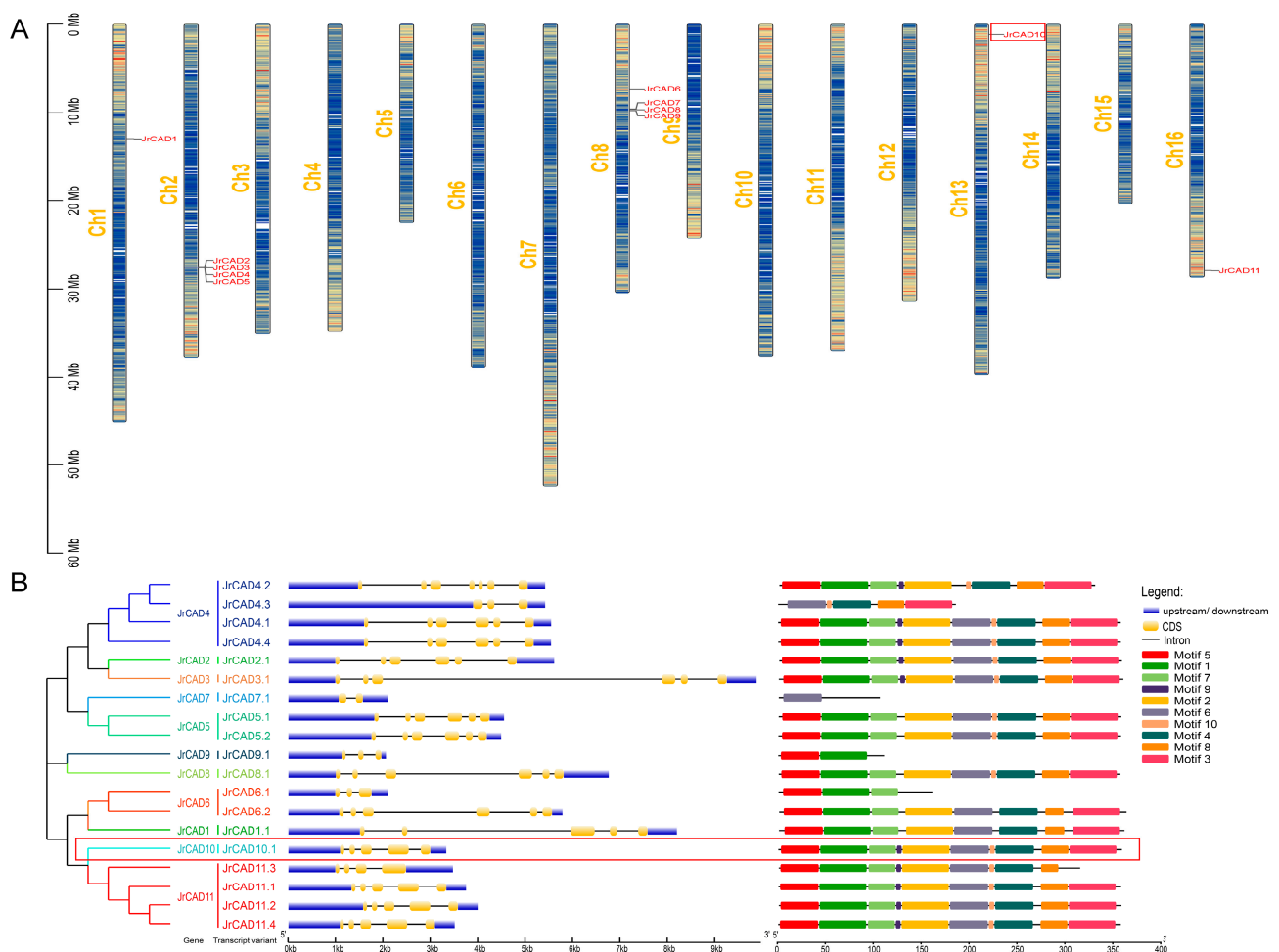


Figure 3. Bioinformatics analysis of walnut *JrCAD* genes. (A) Chromosomal localization of *JrCAD* genes. Mb: megabase. (B) Structural, evolutionary, and conserved motif analysis of *JrCAD* genes. upstream/downstream: 5' and 3' non-coding regions of the gene; CDS: coding sequence; Kb: kilobase.

An evolutionary analysis of the amino acid sequences of the 11 *JrCAD*s showed that the *JrCAD* family members of “Xinlu” walnuts can be divided into three classes, including Class I, Class II, and Class III. Class I includes five members, *JrCAD2*, *JrCAD3*, *JrCAD4*, *JrCAD5*, and *JrCAD7*. Class II has only two members, *JrCAD8* and *JrCAD9*. Class III comprises four members, *JrCAD1*, *JrCAD6*, *JrCAD10*, and *JrCAD11*. An analysis revealed that *JrCAD1*, *JrCAD2*, *JrCAD3*, *JrCAD7*, *JrCAD8*, *JrCAD9*, and *JrCAD10* have unique transcripts in the endocarp of “Xinlu” walnuts, which may suggest that these genes perform relatively conserved and singular functions. However, it was found that *JrCAD4*, *JrCAD5*, *JrCAD6*, and *JrCAD11* possess multiple splice variants. These genes may exert different functions by forming distinct transcripts through alternative splicing. A total of 10 motifs were identified among the 11 *JrCAD* members. *JrCAD7* was found to possess the fewest motifs, containing only Motif 6. *JrCAD2.1*, *JrCAD3.1*, *JrCAD4.1*, *JrCAD4.4*, *JrCAD10.1*, *JrCAD11.1*, *JrCAD11.2*, and *JrCAD11.4* were found to have all the conserved motifs (Motif 1 to Motif 10). *JrCAD4.2* was found to lack Motif 6. *JrCAD4.3* was found to be missing Motif 1, Motif 2, Motif 5, Motif 7, and Motif 9. *JrCAD5.1*, *JrCAD5.2*, and *JrCAD8.1* were all found to lack Motif 9. *JrCAD6.1* was found to contain Motif 1, Motif 5, and Motif 7. *JrCAD1.1* and *JrCAD6.2* were found to be missing Motif 9 and Motif 10. *JrCAD9.1* was found to contain Motif 1 and Motif 5. *JrCAD11.3* was found to be missing Motif 3. The diverse *JrCAD* family members and complex splice variants may play diversified roles in the development of the endocarp of “Xinlu” walnuts.

3.5. Analysis of the Lignin Biosynthetic Pathway in “Xinlu” Walnuts

To further identify the key genes involved in lignin biosynthesis, we summarized the lignin biosynthetic pathway in the endocarp of “Xinlu” walnuts based on the phenylpropanoid metabolism information from the KEGG website (Figure 4).

The first step in lignin biosynthesis involves the deamination of phenylalanine by phenylalanine ammonia-lyase (PAL) to produce cinnamic acid. Subsequently, cinnamic acid undergoes a series of enzymatic reactions catalyzed by cinnamate 4-hydroxylase (C4H), coumarate 3-hydroxylase (C3H), caffeic acid O-methyltransferase (COMT), and ferulate-5-hydroxylase (F5H) to generate various derivative acids (acid units). It could be observed that 4CL is an essential gene in the phenylpropanoid metabolism pathway and the final node connecting the phenylpropanoid metabolism pathway to downstream metabolic pathways. Its enzymatic catalysis involves the binding of various coumaric acids and derived acids in acid units with coenzyme A to form corresponding acid-CoA products, such as coumaroyl-CoA (Figure 4A). These coenzyme A products are catalyzed by different enzymes to activate other metabolic pathways. When catalyzed by the CCR enzyme, these coenzyme A products enter the lignin biosynthetic pathway to form corresponding aldehyde substances. These aldehyde substances produce the three basic monomers of lignin synthesis p-coumaryl alcohol, coniferyl alcohol, and sinapyl alcohol under the action of CAD enzymes. The three critical hub genes, *Jr4CL*, *JrCCR*, and *JrCAD10*, occupy key positions in the lignin biosynthesis pathway, primarily regulating lignin production and the G/S ratio of lignin. In the endocarp of “Xinlu” walnuts, it was found that the contents of p-coumaryl alcohol, coniferyl alcohol, and sinapyl alcohol in the PUH were significantly lower than those in the SCH ($p < 0.01$), especially the content of sinapyl alcohol, which was undetectable in the PUH. During the StE stage, the content of p-coumaryl alcohol in the SCH was 11.2 times higher than that in the PUH. The synthesis of coniferyl alcohol was significantly inhibited in the PUH, with its content decreasing from 2,094,000 to 1,218,000. The sinapyl alcohol content in the SCH increased from 15,660 to 34,800, then decreased to 23,180, and finally increased again to 36,900 (Figure 4B). We extracted six mRNAs of *Jr4CL*, three mRNAs of *JrCCR*, and four mRNAs of *JrCAD* from 14 LIG-related modules in “Xinlu” walnuts. The clustering of samples indicates that the expression levels of *Jr4CL*, *JrCCR*, and *JrCAD* in the SCH were significantly higher than those in the PUH. Based on the analysis of transcript expression levels, it was found that except for *Jr4CL-MXL.17872*

and *Jr4CL-MXL.27747*, the expression levels of the other 11 mRNAs in the SCH were higher than those in the PUH (Figure 4C).

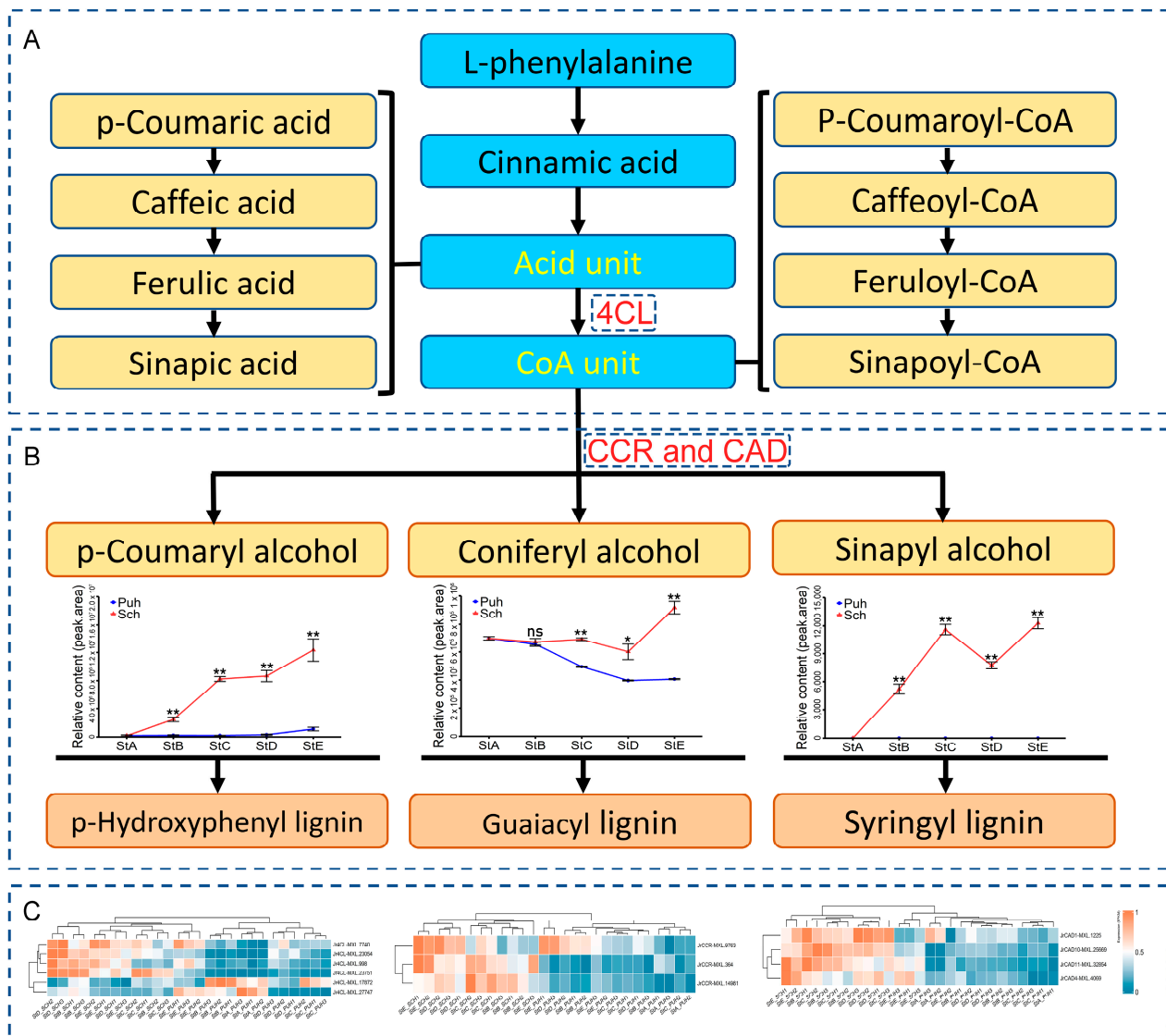


Figure 4. Lignin biosynthesis in “Xinlu” walnuts. (A) Phenylpropanoid metabolic pathway. 4CL: cinnamate 4-hydroxylase. (B) Lignin biosynthetic pathway. CCR: cinnamoyl-CoA reductase; CAD: cinnamyl alcohol dehydrogenase. StA means 50 days after peak blooming (DAF), StB means 64 DAF, StC means 71 DAF, StD means 78 DAF, and StE means 92 DAF. Scleritic-hue (SCH) is the hardened, shell-like area in which lignification has taken place, and pulpy-hue (PUH) is the unligified fleshy portion. The asterisk denotes a significant difference between the walnut PUH and SCH in the same period, as determined using Student’s *t*-test. * $p < 0.05$, ** $p < 0.01$; ns indicates no significant difference. (C) Expression clustering heatmap of key hub genes. In the heatmap, the rows represent genes, while the columns represent samples.

3.6. Expression Analysis of *JrCAD10* during Different Developmental Stages of Walnut Fruit and in Various Walnut Tissues

To analyze the expression pattern of *JrCAD10* during the different developmental stages of “Xinlu” walnut fruits and in different tissues of “Xinlu” walnuts, we performed fluorescent quantitative PCR on *JrCAD10*, a key hub gene for lignin biosynthesis, and we calculated the RCN based on the reference gene *LOC121245754*.

The results of the analysis showed that the expression level of *JrCAD10* was the lowest in the exocarp of “Xinlu” walnuts, with an RCN of 0.32. The highest expression level of *JrCAD10* was observed in the SCH, with an RCN of 3.2. The expression level of *JrCAD10* in the SCH was 10 times higher than that in the exocarp. Among the different tissues of “Xinlu” walnuts, the expression level of *JrCAD10* in the SCH was significantly higher than that in all other tissues, and there was no significant difference in *JrCAD10* expression among all other tissues, except for in the SCH ($p < 0.01$) (Figure 5A). At StD, the expression levels of *JrCAD10* reached their peak in both SCH and PUH, with RCN values of 7.5 and 2.2, respectively. From the StA to StB stage of endocarp development in “Xinlu” walnuts, the expression level of *JrCAD10* in the SCH rapidly increased, exhibiting an “M”-shaped trend. In contrast, the expression level of *JrCAD10* in the PUH showed little fluctuation. From the StB to StE stage, the expression level of *JrCAD10* in the SCH was significantly higher than that in the PUH ($p < 0.01$) (Figure 5B). Furthermore, there was consistency between the *JrCAD10* expression patterns observed in the qRT-PCR data and those observed in the RNA-Seq data, with a Pearson correlation coefficient of 0.783, indicating the reliability of our omics sequencing data (Supplementary Material Table S3). Our analysis indicates that *JrCAD10* positively regulates the lignification of the endocarp in “Xinlu” walnuts. It is highly expressed only in the SCH of the endocarp of “Xinlu” walnuts and has a significant impact on lignin production.

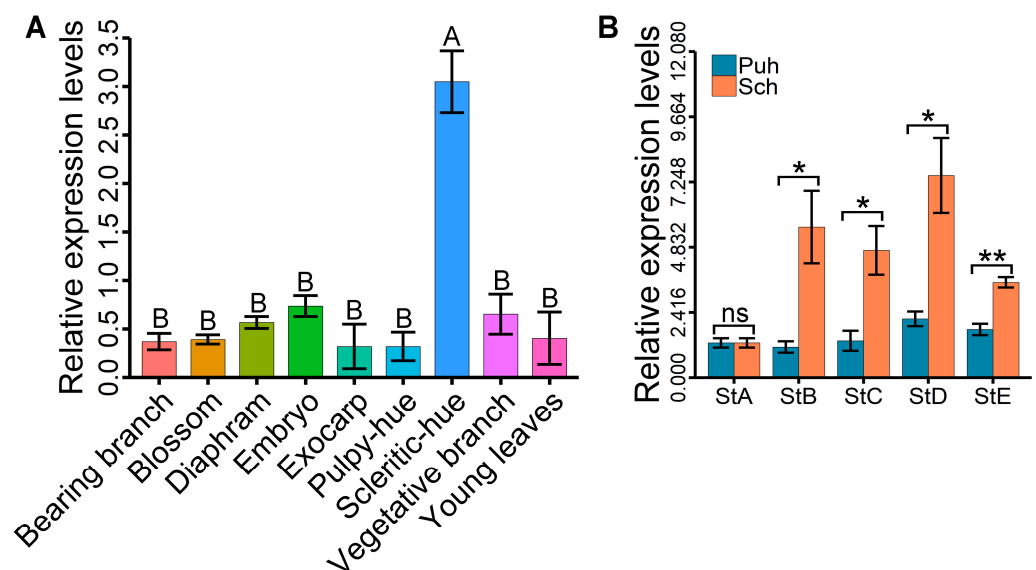


Figure 5. The relative gene expression patterns of *JrCAD10* in the Puh and Sch of “Xinlu” walnuts. (A) The relative expression levels of *JrCAD10* in different tissues of “Xinlu” walnuts. (B) The relative expression levels of *JrCAD10* during different developmental stages of the endocarp in “Xinlu” walnuts. StA means 50 days after peak blooming (DAF), StB means 64 DAF, StC means 71 DAF, StD means 78 DAF, and StE means 92 DAF. Scleritic-hue (SCH) is the hardened, shell-like area in which lignification has taken place, and pulpy-hue (PUH) is the unlignified fleshy portion. The data represent the mean \pm SD. The asterisk denotes a significant difference between the walnut PUH and SCH in the same period, as determined using Student’s *t*-test. * $p < 0.05$, ** $p < 0.01$; ns indicates no significant difference. Uppercase letters indicate significant differences among different tissues of “Xinlu” walnuts, as determined using the SNK test ($p < 0.01$). Error bars represent the standard error of 3 biological replicates.

4. Discussion

In recent years, propelled by market forces, the walnut industry has undergone a notable transformation, evolving from primary to deep processing. This paradigm shift has led to increased demands on the quality of walnut raw materials, driven by the need to minimize production costs and mitigate industrial waste, particularly in the form of

crushed walnut shells. As a result, thin-shelled or shell-less bared-nut walnuts, commonly known as “Xinlu”, have emerged as a potentially significant option for the deep-processing industry. This study utilizes this unique cultivar due to its distinctive characteristic of abnormally developed endocarps, specifically characterized by a lack of lignification or minimal lignification in the PUH, rendering it incapable of forming hard shell tissue.

It is widely recognized that the structure of an actual fruit’s pericarp typically comprises three layers, namely, the exocarp, mesocarp, and endocarp, which are derived directly from the ovary wall (as seen in fruits such as apricots, peaches, and plums). These layers exhibit marked structural differences and play distinct physiological roles. The exocarp serves as a barrier against external pathogens, while the endocarp undergoes lignification to form a hard shell, shielding the seeds from physical, chemical, and biological threats. We classify the walnut fruit as a pseudocarp due to the fusion of its floral receptacle, calyx, and ovary in its development. This classification aligns with previous conclusions that the walnut is a drupe-like fruit [15]. Although the structure of the walnut pericarp is similar to that of actual fruits (Figure 1A), their developmental origins differ entirely. The exocarp and mesocarp of walnuts are derived from the receptacle and calyx tissues. In contrast, the exocarp and mesocarp of actual fruits originate from the outer and middle walls of the ovary. In walnuts, the hardening of the endocarp initially occurs in the apical region and then rapidly progresses along the suture lines, with cells perpendicular to the suture lines hardening at a slower rate [13]. Our results indicate that the hardening of the endocarp in walnuts initiates in both the apical and basal regions and progresses towards the central region of the fruit (Figure 1A), slightly differing from the results of previous research. This is different from our previous conclusion that lignin accumulates in a short period of time to form a complete hard shell in paper skin peach [21]. The reason for this may be the difference in lignin deposition patterns in the endocarp of different walnut varieties.

The thickness and hardness of walnut shells are two important quality indicators that significantly impact walnut processing and the consumer’s eating experience. The thickness of the walnut shell directly affects the ease of shelling. A thicker shell means that more force and time are required to crack it, which can lead to inefficient processing and higher costs. The hardness of the walnut shell determines the integrity of the kernel during the shelling process. A hard shell may damage the kernel when cracked, resulting in broken or fragmented kernels, which not only reduces the eating quality of the kernel but also affects its commercial value. Lignin is an essential component of plant cell walls, particularly in secondary cell walls. It is a complex organic polymer formed through enzymatic polymerization reactions of phenolic monomers, primarily p-coumaryl alcohol, coniferyl alcohol, and sinapyl alcohol [32]. Some scholars have demonstrated that the thickness and hardness of walnut shells increase with the lignin content [33]. In a study examining the lignin composition of Tartary buckwheat seed shells, there was a strong negative correlation found between the hardness of the seed shells and the S-lignin content [34]. Our findings revealed that the lignin in the endocarp of “Xinlu” walnuts undergoes rapid synthesis and accumulation within just 1–2 weeks from the onset of synthesis, followed by a gradual change in the lignin content within the already lignified walnut SCH (Figure 1B). These observations align with those of previous research [13]; nevertheless, the rapid synthesis and accumulation of lignin within this short timeframe do not necessarily correlate with the development of complete hard shells in “Xinlu” walnut fruits (Figure 1A,B).

Lignin biosynthesis is influenced by numerous structural genes in the phenylpropanoid metabolism pathway. The upregulation or silencing of genes such as *PAL*, *C3H*, *C4H*, and *CCoAOMT* can lead to changes in lignin content and structure [35–38]. We found that sinapyl alcohol undergoes significant accumulation in the SCH from the StA to StE stages while remaining undetectable in the PUH (Table 1). Therefore, we measured the transcriptomes of “Xinlu” walnut endocarps at various developmental stages to investigate the key hub genes and molecular regulatory networks involved in sinapyl alcohol biosynthesis at the transcriptional level. Based on a WGCNA analysis, we identified 14 modules significantly associated with LIG (Figure 2A) and identified *JrCAD10* as a key gene.

Additionally, we established a co-expression network of genes in the MEplum3 module, revealing the lignin biosynthetic pathway. Within this pathway, *JrCCR* and *JrCAD10* emerged as two prominent hub genes (Figure 2D). Previous research indicates that inhibiting *CCR* and *CAD* expression can lead to a decrease in lignin content and alterations in its structure [39,40]. Therefore, the absence of sinapyl alcohol in the PUH may result in a reduced lignin content and significantly modify the composition of the lignin structure. In addition, from StD to StE, metabolites such as cellulose, hemicellulose, lignin, p-coumaryl alcohol, coniferyl alcohol, and sinapyl alcohol in the endocarp of “Xinlu” walnuts all showed an upward or rapid upward trend. This may be the result of the lignification of the diaphragm tissue close to the inside of the endocarp during this period [21].

This study described the transcriptional changes in hub genes and variations in lignin metabolism related to the development of the walnut endocarp. We constructed 27 samples across five developmental stages, obtaining high-quality transcriptome and lignin metabolome datasets. Through a comprehensive analysis of the phenylpropanoid metabolism and lignin biosynthesis pathway during the development of the walnut endocarp, we successfully identified the dynamic expression patterns of the key hub gene *JrCAD10* in different walnut tissues and at various stages of fruit development. Our findings provide novel insights into the regulatory mechanisms underlying lignin biosynthesis and offer a plausible explanation for the formation of the PUH in “Xinlu” walnuts. Moreover, our findings have the potential to facilitate advancements in walnut gene modification and contribute significantly to the breeding and utilization of walnuts for future deep-processing industries.

5. Conclusions

The biosynthesis of lignin is inhibited during the development of the endocarp in “Xinlu” walnuts, leading to the formation of a PUH in the endocarp. Severe reductions in the contents of lignin biosynthesis monomers, including p-coumaryl alcohol, coniferyl alcohol, and sinapyl alcohol, are the primary reasons for the inhibition of lignin biosynthesis during the development of the endocarp in “Xinlu” walnuts. The expression of key genes, such as *JrCAD10*, which are involved in lignin biosynthesis during the development of the endocarp in “Xinlu” walnuts, is severely suppressed. This suppression is the main cause of the severe reductions in p-coumaryl alcohol, coniferyl alcohol, and sinapyl alcohol contents. The PUH of the endocarp in “Xinlu” walnuts gradually loses water, shrinks, and ruptures during the later stages of fruit ripening, ultimately leading to the formation of a bared-nut walnut.

Supplementary Materials: The following supporting information can be downloaded at <https://www.mdpi.com/article/10.3390/horticulturae10050487/s1>: Table S1: Summary of qRT-PCR primers employed in the present study; Table S2: Comparison of differences in lignin metabolites; Table S3: Transcriptome and qRT-PCR-Pearson correlation coefficient of *JrCAD10*; Table S4: Summary of gene expression levels in the endocarp of walnuts at five developmental stages; Table S5: Summary of mRNA expression levels in the endocarp of walnuts across five developmental stages; Table S6: Summary of transcriptome annotation of walnut endocarp at five developmental stages; Figure S1: Sample clustering and trait heatmap of walnut endocarp at five developmental stages.

Author Contributions: Conceptualization, R.Z., Q.J., H.H. and J.B.; methodology, R.Z. and S.Y.; software, S.Y.; validation, R.Z., S.Y. and Q.J.; formal analysis, S.Y. and J.F.; investigation, S.Y., Q.Y. and J.F.; resources, H.H.; data curation, S.Y.; writing—original draft preparation, S.Y.; writing—review and editing, Q.Y. and P.W.; visualization, S.Y.; supervision, R.Z., Q.J. and Z.G.; project administration, R.Z. and Z.G.; funding acquisition, R.Z. All authors have read and agreed to the published version of the manuscript.

Funding: This research work was supported by the National Natural Science Foundation of China (32160698); the South Xinjiang Key Industry Innovation Development Support Program (2022DB022); the Tarim University Scientific Research Innovation Project (XJ2022G238); the “Tianshan Talents” Training Program for Young Top-notch Scientific Talents focused on Walnut Germplasm Resources Collection, Evaluation, Creation, and Characteristic Hard Shell Development Research; and the South Xinjiang Horticultural Research Center Scientific Research Condition Construction Project (TDZKKY202204), laying a solid foundation for the research conducted.

Data Availability Statement: The data supporting this study’s findings are available on request from the corresponding author. The data are not publicly available due to privacy and ethical restrictions.

Acknowledgments: All authors would like to express their gratitude to Zhiyong Pan (from Huazhong Agricultural University, China) for his generous funding support of the project and to Zhengyan Fan (from Institute of Fruit Tree Research, Guangdong Academy of Agricultural Sciences, China) for providing invaluable technical assistance.

Conflicts of Interest: The authors declare no conflicts of interest.

References

- Bernard, A.; Lheureux, F.; Dirlwanger, E. Walnut: Past and future of genetic improvement. *Tree Genet. Genomes* **2017**, *14*, 6–28. [\[CrossRef\]](#)
- Zhang, J.; Zhang, W.; Ji, F.; Qiu, J.; Song, X.; Bu, D.; Pan, G.; Ma, Q.; Chen, J.; Huang, R.; et al. A high-quality walnut genome assembly reveals extensive gene expression divergences after whole-genome duplication. *Plant Biotechnol. J.* **2020**, *18*, 1848–1850. [\[CrossRef\]](#) [\[PubMed\]](#)
- Zhou, Y.; Wang, D.; Niu, F. Studies on constituents from pericarps of *Juglans mandshurica* with anti-tumor activity. *Chin. Tradit. Herb. Drugs* **2010**, *41*, 11–14.
- Ji, Y.; Ma, H.; Yang, B.; Ji, C. Antitumor effects of different extract fractions from Qinglongyi. *Chin. Tradit. Herb. Drugs* **2004**, *35*, 71–73.
- Huimin, T.; Liju, Z. Ultrasound-assisted cellulase extraction of polysaccharide from walnut shell and its antioxidant activity. *China Oils Fats* **2020**, *45*, 101–105.
- Fordos, S.; Abid, N.; Gulzar, M.; Pasha, I.; Fatih, O.; Shahid, A.; Khan, M.K.I.; Mousavi Khaneghah, A.; Aadil, R.M. Recent development in the application of walnut processing by-products (walnut shell and walnut husk). *Biomass Convers. Biorefin.* **2023**, *13*, 14389–14411. [\[CrossRef\]](#)
- Ali, J.-E.; Alireza, O.; Mahnaz, T.; Ryszard, A. A Comprehensive Review on the Chemical Constituents and Functional Uses of Walnut (*Juglans* spp.) Husk. *Int. J. Mol. Sci.* **2019**, *20*, 3920. [\[CrossRef\]](#) [\[PubMed\]](#)
- Sheng, F.; Hu, B.; Jin, Q.; Wang, J.; Wu, C.; Luo, Z. The Analysis of Phenolic Compounds in Walnut Husk and Pellicle by UPLC-Q-Orbitrap HRMS and HPLC. *Molecules* **2021**, *26*, 3013. [\[CrossRef\]](#) [\[PubMed\]](#)
- Hardman, W.E. Walnuts Have Potential for Cancer Prevention and Treatment in Mice. *J. Nutr.* **2014**, *144*, 555S–560S. [\[CrossRef\]](#)
- Bhooshan, P.K.; Ibrahim, R.S. Plant Polyphenols as Dietary Antioxidants in Human Health and Disease. *Oxid. Med. Cell. Longev.* **2009**, *2*, 270–278.
- Jia, X.; Luo, H.; Xu, M.; Zhai, M.; Wang, L. Dynamic Changes in Phenolics and Antioxidant Capacity during Pecan (*Carya illinoensis*) Kernel Ripening and Its Phenolics Profiles. *Molecules* **2018**, *23*, 435. [\[CrossRef\]](#) [\[PubMed\]](#)
- Qiang, J.; Shan, G.; Rongli, M.; Fang, S.; Qinglin, Z.; Cuiyun, W.; Rui, Z.; Zhengrong, L. A Preliminary Study for Identifying Genes Associated with Pellicle Development in Xinjiang Walnut (*Juglans regia* L.). *Horticulturae* **2022**, *8*, 784. [\[CrossRef\]](#)
- Pinney, K.; Polito, V.S. English walnut fruit growth and development. *Sci. Hortic.* **1983**, *21*, 19–28. [\[CrossRef\]](#)
- Zhifeng, Z.; Juchun, Z.; Bo, H.; Hongjian, Z.; Rong, W. Study on the Constituents of Walnut Shell. *J. Southwest For. Univ.* **2006**, *26*, 33–36.
- Ling, X.; Yaoping, X.; Xiangui, Z.; Jihua, L. The Developmental Anatomy on the Pericarp of *Juglans Regia*. *Acta Bot. Boreali-Occident. Sin.* **1998**, *18*, 577–580.
- Li, X.B.; Zhao, S.G.; Wang, H.X.; Gao, Y.; Zhang, Z.H. Relationship between Walnut Shell Structures and the Content of Lignin and Cellulose. *Hubei Agric. Sci.* **2012**, *51*, 5076–5079.
- Coleman, H.D.; Park, J.Y.; Nair, R.; Chapple, C.; Mansfield, S.D. RNAi-mediated suppression of p-coumaroyl-CoA 3'-hydroxylase in hybrid poplar impacts lignin deposition and soluble secondary metabolism. *Proc. Natl. Acad. Sci. USA* **2008**, *105*, 4501–4506. [\[CrossRef\]](#) [\[PubMed\]](#)
- Lu, F.; Marita, J.M.; Lapierre, C.; Jouanin, L.; Morreel, K.; Boerjan, W.; Ralph, J. Sequencing around 5-Hydroxyconiferyl Alcohol-Derived Units in Caffeic Acid O-Methyltransferase-Deficient Poplar Lignins. *Plant Physiol.* **2010**, *153*, 569–579. [\[CrossRef\]](#)
- Nakashima, J.; Chen, F.; Jackson, L.; Shadle, G.; Dixon, R.A. Multi-site genetic modification of monolignol biosynthesis in alfalfa (*Medicago sativa*): Effects on lignin composition in specific cell types. *New Phytol.* **2010**, *179*, 738–750. [\[CrossRef\]](#)
- Rui, Z.; Yan, T.; Hong, Z.; Qiang, J.; Chongzhi, X.; Shan, G.; Hongbo, S. Dynamic-changing Characteristics of 3 Key Secondary Enzymes between Bared- and Completed- Endocarp Development in Walnuts. *Pak. J. Agric. Sci.* **2017**, *54*, 57–63.

21. Yu, S.; Jia, C.; Song, Y.; Liu, C.; Guo, Y.; Zhang, W.; Chen, L.; Zhang, R. Screening and functional prediction of differential expression genes at lignification stage of endocarp in ‘Zhipi’ walnut. *J. Fruit Sci.* **2019**, *36*, 410–420.
22. McKenna, A.; Hanna, M.; Banks, E.; Sivachenko, A.; Cibulskis, K.; Kernytisky, A.; Garimella, K.; Altshuler, D.; Gabriel, S.; Daly, M.; et al. The Genome Analysis Toolkit: A MapReduce framework for analyzing next-generation DNA sequencing data. *Genome Res.* **2010**, *20*, 1297–1303. [[CrossRef](#)] [[PubMed](#)]
23. Kim, D.; Langmead, B.; Salzberg, S.L. HISAT: A fast spliced aligner with low memory requirements. *Nat. Methods* **2015**, *12*, 357–360. [[CrossRef](#)] [[PubMed](#)]
24. Pertea, M.; Pertea, G.M.; Antonescu, C.M.; Chang, T.C.; Mendell, J.T.; Salzberg, S.L. StringTie enables improved reconstruction of a transcriptome from RNA-seq reads. *Nat. Biotechnol.* **2015**, *33*, 290–295. [[CrossRef](#)] [[PubMed](#)]
25. Langmead, B.; Salzberg, S.L. Fast gapped-read alignment with Bowtie 2. *Nat. Methods* **2012**, *9*, 357–359. [[CrossRef](#)] [[PubMed](#)]
26. Dewey, C.N.; Bo, L. RSEM: Accurate transcript quantification from RNA-Seq data with or without a reference genome. *BMC Bioinform.* **2011**, *12*, 323.
27. Lei, K.; Yong, Z.; Zhiqiang, Y.; Xiaoqiao, L.; Shuqi, Z.; Liping, W.; Ge, G. CPC: Assess the protein-coding potential of transcripts using sequence features and support vector machine. *Nucleic Acids Res.* **2007**, *35*, W345–W349.
28. Sun, L.; Luo, H.; Bu, D.; Zhao, G.; Yu, K.; Zhang, C.; Liu, Y.; Chen, R.; Zhao, Y. Utilizing sequence intrinsic composition to classify protein-coding and long non-coding transcripts. *Nucleic Acids Res.* **2013**, *41*, e166. [[CrossRef](#)] [[PubMed](#)]
29. Finn, R.D.; Coghill, P.; Eberhardt, R.Y.; Eddy, S.R.; Mistry, J.; Mitchell, A.L.; Potter, S.C.; Punta, M.; Qureshi, M.; Sangrador-Vegas, A.; et al. The Pfam protein families database: Towards a more sustainable future. *Nucleic Acids Res.* **2016**, *44*, D279–D285. [[CrossRef](#)]
30. Chen, C.; Wu, Y.; Li, J.; Wang, X.; Zeng, Z.; Xu, J.; Liu, Y.; Feng, J.; Chen, H.; He, Y.; et al. TBtools-II: A “one for all, all for one” bioinformatics platform for biological big-data mining. *Mol. Plant* **2023**, *16*, 1733–1742. [[CrossRef](#)]
31. Hu, B.; Jin, J.; Guo, A.Y.; Zhang, H.; Luo, J.; Gao, G. GSDS 2.0: An upgraded gene feature visualization server. *Bioinformatics* **2015**, *31*, 1296–1297. [[CrossRef](#)] [[PubMed](#)]
32. Lin, J.; Wu, H.; Xu, H.; Zhao, Y.; Guo, Y. Plant lignification and its regulation. *Sci. Sin. Vitae* **2020**, *50*, 111–122. [[CrossRef](#)]
33. Xiao, N.; Bock, P.; Antreich, S.J.; Staedler, Y.M.; Schönenberger, J.; Gierlinger, N. From the Soft to the Hard: Changes in Microchemistry During Cell Wall Maturation of Walnut Shells. *Front. Plant Sci.* **2020**, *11*, 466. [[CrossRef](#)] [[PubMed](#)]
34. Yang, W.; Duan, H.; Yu, K.; Hou, S.; Kang, Y.; Wang, X.; Hao, J.; Liu, L.; Zhang, Y.; Luo, L.; et al. Integrative Dissection of Lignin Composition in Tartary Buckwheat Seed Hulls for Enhanced Dehulling Efficiency. *Adv. Sci.* **2024**, *2024*, 2400916. [[CrossRef](#)] [[PubMed](#)]
35. Blee, K.; Choi, J.W.; O’Connell, A.P.; Jupe, S.C.; Schuch, W.; Lewis, N.G.; Bolwell, G.P. Antisense and sense expression of cDNA coding for CYP73A15, a class II cinnamate 4-hydroxylase, leads to a delayed and reduced production of lignin in tobacco. *Phytochemistry* **2001**, *57*, 1159. [[CrossRef](#)] [[PubMed](#)]
36. Lukacin, R.; Matern, U.; Specker, S.; Vogt, T. Cations modulate the substrate specificity of bifunctional class I O-methyltransferase from *Ammi majus*. *FEBS Lett.* **2004**, *577*, 367–370. [[CrossRef](#)]
37. Reddy, M.S.; Chen, F.; Shadle, G.; Jackson, L.; Aljoe, H.; Dixon, R.A. Targeted down-regulation of cytochrome P450 enzymes for forage quality improvement in alfalfa (*Medicago sativa* L.). *Proc. Natl. Acad. Sci. USA* **2005**, *102*, 16573–16578. [[CrossRef](#)]
38. Korth, K.L.; Blount, J.W.; Chen, F.; Rasmussen, S.; Lamb, C.; Dixon, R.A. Changes in phenylpropanoid metabolites associated with homology-dependent silencing of phenylalanine ammonia-lyase and its somatic reversion in tobacco. *Physiol. Plant.* **2001**, *111*, 137–143. [[CrossRef](#)]
39. Ralph, J.; Hatfield, R.D.; Piquemal, J.; Yahiaoui, N.; Pean, M.; Lapierre, C.; Boudet, A.M. NMR characterization of altered lignins extracted from tobacco plants down-regulated for lignification enzymes cinnamylalcohol dehydrogenase and cinnamoyl-CoA reductase. *Proc. Natl. Acad. Sci. USA* **1998**, *95*, 12803–12808. [[CrossRef](#)]
40. Thevenin, J.; Pollet, B.; Letarnec, B.; Saulnier, L.; Gissot, L.; Maia-Grondard, A.; Lapierre, C.; Jouanin, L. The Simultaneous Repression of CCR and CAD, Two Enzymes of the Lignin Biosynthetic Pathway, Results in Sterility and Dwarfism in *Arabidopsis thaliana*. *Mol. Plant* **2011**, *4*, 70–82. [[CrossRef](#)]

Disclaimer/Publisher’s Note: The statements, opinions and data contained in all publications are solely those of the individual author(s) and contributor(s) and not of MDPI and/or the editor(s). MDPI and/or the editor(s) disclaim responsibility for any injury to people or property resulting from any ideas, methods, instructions or products referred to in the content.